JOURNAL OF AIRCRAFT
Vol. 41, No. 2, March–April 2004

Detached-Eddy Simulation of the F-15E at High Alpha

James R. Forsythe*
U.S. Air Force Academy, Colorado Spring, Colorado 80840
Kyle D. Squires†
Arizona State University, Tempe, Arizona 85287
Kenneth E. Wurtzler‡
Cobalt Solutions, LLC, Cincinnati, Ohio 45209
and
Philippe R. Spalart§
Boeing Commercial Airplanes, Seattle, Washington 98124

Detached-eddy simulation (DES) is used to predict the massively separated flow around an F-15E at 65-deg angle of attack. The calculations are performed at flight conditions corresponding to a chord-based Reynolds number of 13.6×10^6 and Mach number of 0.3. Flowfield solutions are obtained using unstructured grids with the commercial solver Cobalt: the average mesh spacing from solid surfaces to the first cell center from the wall under one viscous unit. The influence of the mesh size is assessed using a series of three grids ranging from 2.85×10^6 cells to 10×10^6 cells. In addition, the influence of the time step is investigated using three simulations with varied time steps. DES predictions are assessed via comparison to Boeing's stability and control database as well as to solutions of the Reynolds-averaged Navier–Stokes (RANS) equations. These are steady, with the Spalart–Allmaras model. Both RANS and DES predictions of integrated forces exhibit a relatively weak dependence on the grid density for the range examined. In the DES the wake region is characterized by complex and chaotic three-dimensional structures with direct resolution of a reasonable range of length and timescales. In general, both RANS and DES predictions of averaged quantities exhibit favorable agreement with the database. DES predictions of the lift, drag, and pitching moment, which were averaged over as many as 150 inertial timescales, agree with the data more favorably than the RANS results, but both methods are within 10% of the database. The cost of DES was approximately seven times higher than the steady RANS calculations on the same grid.

Introduction

NUMERICAL simulation of the flow around complex configurations offers a powerful tool for analysis, for example, a means to screen configurations prior to costly and time-consuming flight tests or even wind-tunnel work. One example is in spin testing in which computational fluid dynamics (CFD) will sooner or later be used to provide detailed information on stability, spin modes, etc. Such information could be difficult or impossible to extract from flight tests, and a numerical tool would be clearly useful. Although the overarching goal of the current research is development of a CFD tool for spin analysis, aircraft spin strongly challenges numerical models. The flowfields encountered are three-dimensional, massively separated, and unsteady. In addition, because Reynolds-number effects are important for spin testing, calculations should ideally be performed at flight conditions (although the present geometry is among the more forgiving ones for Reynolds number).

The current effort focuses on the F-15E because of the availability of an extensive stability and control database (Peters, G., and Walck, K., "Excerpts from the F-15E Stability and Control Database," Personal Communication, Dec. 2000). This database was compiled from an extensive series of flight tests, including spins. Gaps in the flight test were filled in with wind-tunnel testing. In this contribution it is the static aircraft at 65-deg angle of attack that is the primary focus of the calculations because for this angle of attack a clean (no control deflections or stores) F-15E will maintain a stable spin.

The majority of current engineering approaches to prediction of unsteady flows are based on solution of the Reynolds-averaged Navier–Stokes (RANS) equations. The turbulence models employed in RANS methods, in principle, parameterize the entire spectrum of turbulent motions. Although they are often adequate in steady flows with no regions of flow reversal, or possibly exhibiting shallow separations, it appears very likely that RANS turbulence models will be unable to accurately predict phenomena dominating flows characterized by massive separations. Unsteady massively separated flows are characterized by geometry-dependent and three-dimensional turbulent eddies. These eddies, arguably, are what defeats RANS turbulence models of any complexity.

To overcome the deficiencies of RANS models for predicting massively separated flows, Spalart et al.[1] proposed detached-eddy simulation (DES) with the objective of developing a numerically feasible and accurate approach combining the most favorable elements of RANS models and large-eddy simulation (LES). The primary advantage of DES is that it can be applied at high Reynolds numbers as can Reynolds-averaged techniques, but also resolves geometry-dependent, unsteady three-dimensional turbulent motions as in LES. DES predictions to date have been favorable,[2] forming one of the motivations for this research. The specific aims are to apply and assess DES, consistent with the long-term goal of developing a CFD tool for analysis and prediction of aircraft spin. The application under consideration is prediction of the time-dependent flow around a complete aircraft-the F-15E at 65-deg angle of attack. The goal is to assess DES predictions against both measurements and predictions of the same configuration obtained using a RANS turbulence model.

For calculations of complex configurations and at high Reynolds numbers, high-performance computation is essential. In this work solutions of the compressible Navier–Stokes equations on

Presented as Paper 0591-2002 at the Aerospace Sciences Meeting, 2002, Reno, NV, 14 January 2002; received 24 April 2003; revision received 30 June 2003; accepted for publication 1 July 2003.

*Associate Professor, Department of Aeronautics; currently Director of Research, Cobalt Solutions, LLC. Senior Member AIAA.
†Professor, Mechanical and Aerospace Engineering Department. Member AIAA.
‡Director of Operations. Member AIAA.
§Technical Fellow.

unstructured grids are obtained using Cobalt.[3] The numerical method is based on a finite volume approach and is second-order accurate in space and time. The method is point implicit and permits Courant–Friedrichs–Lewy (CFL) numbers as large as 10^6 for steady-state computations.[4] Turbulence-resolving simulations such as DES are necessarily time dependent. For feature-resolving techniques such as DES, important in assessment of the predictions is sensitivity to both mesh resolution and computational timestep. Presented in subsequent sections is a reasonably comprehensive grid and time-step refinement study.

Computational Approach

Spalart–Allmaras Model

The Spalart–Allmaras (S-A) one-equation model[5] solves a single partial differential equation for a variable $\tilde{\nu}$, which is related to the turbulent viscosity. The differential equation is derived by "using empiricism and arguments of dimensional analysis, Galilean invariance and selected dependence on the molecular viscosity."[5] The model includes a wall destruction term that reduces the turbulent viscosity in the log layer and laminar sublayer and trip terms that provide a controlled transition from laminar to turbulent flow. In the present computations the trip term was not active; the transport equation then takes the form,

$$\frac{\mathrm{D}\tilde{\nu}}{\mathrm{D}t} = c_{b1}\tilde{S}\tilde{\nu} - c_{w1}f_w\left[\frac{\tilde{\nu}}{d}\right]^2 + \frac{1}{\sigma}\left\{\nabla\cdot[(\nu+\tilde{\nu})\nabla\tilde{\nu}] + c_{b2}(\nabla\tilde{\nu})^2\right\} \tag{1}$$

The turbulent viscosity is determined via

$$\nu_t = \tilde{\nu}f_{v1}, \qquad f_{v1} = \frac{\chi^3}{\chi^3 + c_{v1}^3}, \qquad \chi \equiv \frac{\tilde{\nu}}{\nu} \tag{2}$$

where ν is the molecular viscosity. Using S to denote the magnitude of the vorticity, the modified vorticity $\tilde{S}$ is defined as

$$\tilde{S} \equiv S + \frac{\tilde{\nu}}{\kappa^2 d^2}f_{v2}, \qquad f_{v2} = 1 - \frac{\chi}{1+\chi f_{v1}} \tag{3}$$

where d is the distance to the closest wall. The wall destruction function f_w is

$$f_w = g\left(\frac{1+c_{w3}^6}{g^6 + c_{w3}^6}\right)^{\frac{1}{6}} \tag{4}$$

with

$$g = r + c_{w2}(r^6 - r), \qquad r \equiv \frac{\tilde{\nu}}{\tilde{S}\kappa^2 d^2} \tag{5}$$

The model constants are given by

$$c_{b1} = 0.1355, \qquad \sigma = \frac{2}{3}, \qquad c_{b2} = 0.622$$
$$\kappa = 0.41, \qquad c_{w1} = \frac{c_{b1}}{\kappa^2} + \frac{(1+c_{b2})}{\sigma}, \qquad c_{w2} = 0.3$$
$$c_{w3} = 2, \qquad c_{v1} = 7.1 \tag{6}$$

Detached-Eddy Simulation

The three-dimensional and time-dependent flow around the F-15E is predicted using detached-simulation. The DES formulation in this study is based on a modification to the S-A RANS model[5] such that the model reduces to its RANS formulation near solid surfaces and to a subgrid model away from the wall.[6] The basis is to attempt to take advantage of the usually adequate performance of RANS models in the thin shear layers where these models are calibrated and the power of LES for resolution of geometry-dependent and large three-dimensional eddies. The DES formulation is obtained by replacing in the S-A model the distance to the nearest wall d by $\tilde{d}$, where $\tilde{d}$ is defined as

$$\tilde{d} \equiv \min(d, C_{\mathrm{DES}}\Delta) \tag{7}$$

In Eq. (7) for the current study, Δ is the largest distance between the cell center under consideration and the cell center of the neighbors (i.e., those cells sharing a face with the cell in question). In "natural" applications of DES, the wall-parallel grid spacings (e.g., streamwise and spanwise) are at least on the order of the boundary-layer thickness, and the S-A RANS model is retained throughout the boundary layer, i.e., $\tilde{d} = d$. Consequently, prediction of boundary-layer separation is determined in the RANS mode of DES. Away from solid boundaries the closure is a one-equation model for the subgrid scale (SGS) eddy viscosity. When the production and destruction terms of the model are balanced, the length scale $\tilde{d} = C_{\mathrm{DES}}\Delta$ in the LES region yields a Smagorinsky eddy viscosity $\tilde{\nu} \propto S\Delta^2$. Analogous to classical LES, the role of Δ is to allow the energy cascade down to the grid size; roughly, it makes the pseudo-Kolmogorov length scale, based on the eddy viscosity, proportional to the grid spacing. The additional model constant $C_{\mathrm{DES}} = 0.65$ was set in homogeneous turbulence[7] and is used without modification in this study.

Numerical Approach

Code Details

The computations were performed using the Cobalt code, a commercial unstructured finite volume method developed for solution of the compressible Navier–Stokes equations and described in Strang et al.[3] The numerical method is a cell-centered finite volume approach applicable to arbitrary cell topologies (e.g, hexahedrals, prisms, tetrahdrons). The spatial operator uses the exact Reimann solver of Gottlieb and Groth,[8] least-squares gradient calculations using QR factorization to provide second-order accuracy in space, and total-variation-diminishing flux limiters to limit extremes at cell faces. A point-implicit method using analytic first-order inviscid and viscous Jacobians is used for advancement of the discretized system. For time-accurate computations a Newton subiteration scheme is employed; the method is second-order accurate in time.

For parallel performance Cobalt utilizes the domain decomposition library ParMETIS[9] to provide optimal load balancing with a minimal surface interface between zones. Communication between processors is achieved using message-passing interface, with parallel efficiencies above 95% on as many as 1024 processors.[10]

In the calculations presented in this manuscript, three Newton subiterations were used for all time-accurate calculations, which roughly doubles the cost of each time step compared to computations of the steady-state solution, but is necessary to ensure time accuracy (steady-state calculations are performed with zero or one subiteration). In addition, to obtain sufficient samples in the averages, statistics were acquired over a minimum of 100 time units (L/V_∞). For a dimensionless time step of 0.014 (nondimensionalized by the chord and the freestream velocity), this required over 7000 time steps. Steady-state RANS calculations required on average about 2000 iterations for convergence. Based on the increased number of subiterations and the larger number of time steps required to obtain a time-averaged solution, DES (or unsteady RANS) cost roughly seven times as much on the same grid as the steady RANS calculations. For example, the baseline grid required 53 seconds per iteration on 128 processors of an IBM P3 for DES (three Newton subiterations). The baseline grid steady RANS calculations (one Newton subiteration) required half the time per time step. This leads to a cost of 13,000 CPU hours for 7000 iterations of DES and 1880 CPU hours for 2000 iterations of steady RANS.

Experience with the simulation technique and flow solver has been developed through previous DES applications to predictions of the flow over a forebody cross section modeled by a rounded-corner square,[11] supersonic axisymmetric base,[12] and section of a NACA 0012 airfoil. Supercritical solutions of the flow over the rounded-corner square agreed well with experimental pressure measurements, in contrast to large errors in RANS and LES calculations.[11]

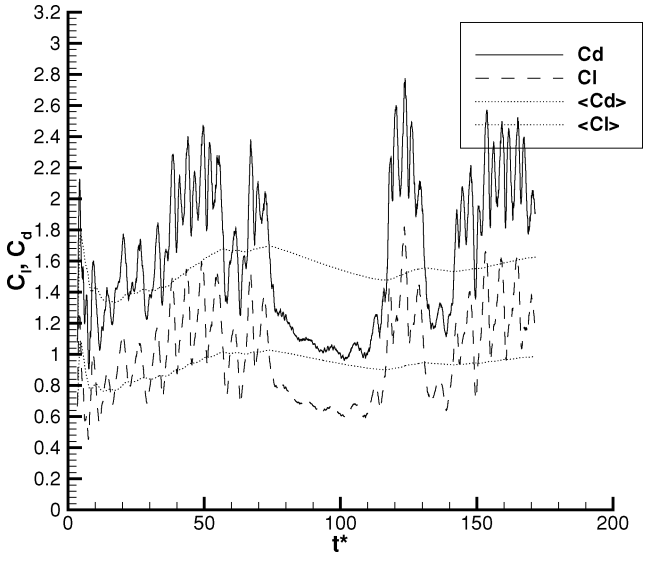

a)

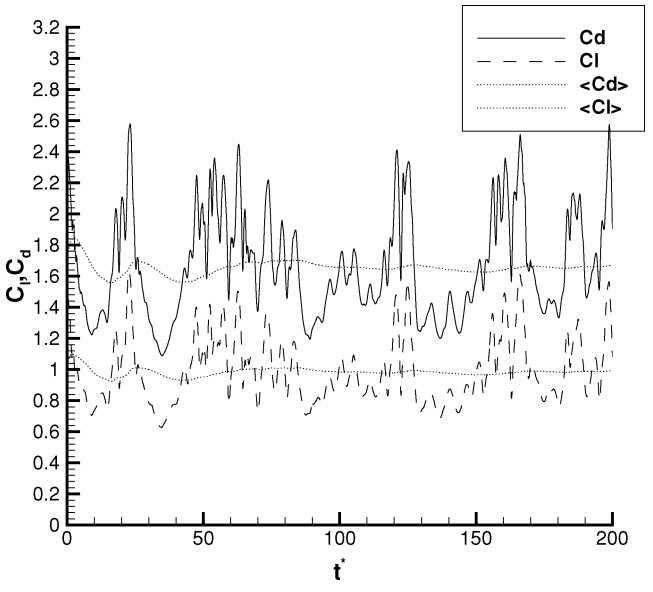

b)

Fig. 1 DES predictions of lift and drag coefficients over the NACA 0012 airfoil section at 60° angle of attack: $Re = 10^5$: a) Cobalt simulation—Instantaneous lift and drag coefficients and running time averages and b) Shur et al.[7] simulation—instantaneous lift and drag on the left and running time average on the right.

DES predictions of the supersonic axisymmetric base flow[12] showed good agreement to experimental base pressures and off-body turbulent kinetic energy. A code-to-code comparison was accomplished through prediction of a NACA 0012 airfoil section. Cobalt calculations were performed using the same grid and with the same time step as in Shur et al.[7] Unsteady lift and drag coefficient histories are shown in Fig. 1 for calculations at a chord-based Reynolds number of 10^5. In both figures the time axis is made dimensionless using the chord length and velocity of the freestream. As shown in the figure, an interesting feature of the lift and drag histories in Shur et al.[7] is the relatively strong modulation of the forces, an effect also produced in the Cobalt solutions. In addition, the mean values for both C_l and C_d agree well between the two calculations.

Grid Generation

A baseline grid was created for a half-aircraft configuration using VGRIDns[13] and is shown in Fig. 2. Using VGRIDns, an initial mesh consisting of 7.9×10^6 tetrahedral cells was generated using the advancing layers (the stretched cells near the surface) and the advancing front methods. Using the Cobalt grid utility blacksmith, nine layers near the wall (generated by the advancing layers method) were combined into prisms, reducing the total number of cells to 5.9×10^6 for the baseline mesh. The distance from solid surfaces to the first cell center normal to the wall was constant, resulting in an average distance measured in wall units of 0.7. Cell growth in the wall-normal direction was specified using a geometric stretching factor of 1.3. There were approximately 1.6×10^5 faces on the surface of the aircraft with only a few hundred cells on the outer boundary. Currently, the engine inlet and exhaust are set to a no-slip boundary condition. At an early phase of the study, modeling the inlet with a mass-flow boundary condition was attempted. For the flow at 65-deg angle of attack, a separation bubble formed, which impinged on the inlet boundary. This in turn lead to numerical instabilities because the flow was both entering and exiting a boundary at which a mass-flow boundary condition was being applied. An important aspect of future work will be extension of the inlet geometry and to model the flow through the engine.

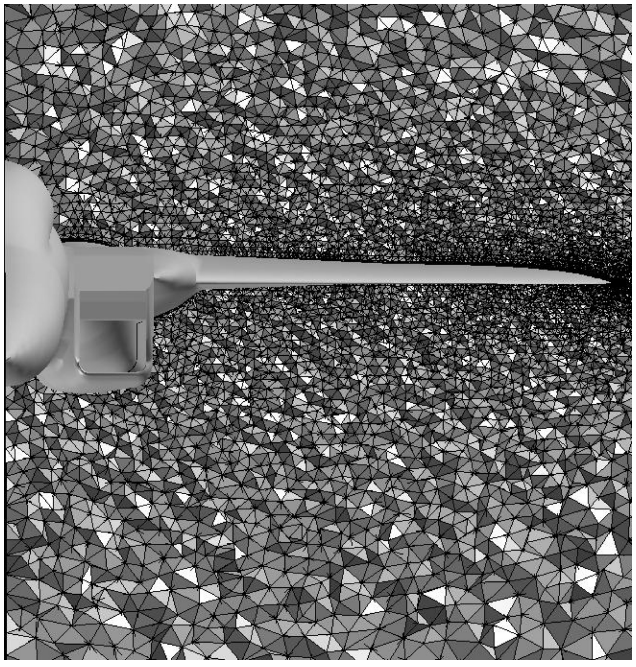

Fig. 2 Baseline computational mesh near aircraft surface.

An advantage of the application of unstructured grids for use in DES is that the tetrahedra outside the boundary layer are nearly isotropic; such cell types are optimal for LES and sometimes difficult to achieve using a structured approach. Isotropic cells ensure the lowest value of Δ for a given cell volume, lowering the eddy viscosity, in turn allowing more fluctuations to be resolved on the mesh. Also, because the orientation of small turbulent structures are not known a priori isotropic cells are a logical approach to representing the eddies.

Sensitivity to the mesh was examined via computations using two additional grids (see Figs. 3–5), one coarser and the other finer than the baseline mesh. Generation of the baseline grid required one week using VGRIDns.[13] Each additional grid was created in one day. VGRIDns uses background sources to define grid spacing. The cell spacing at any location in the grid is a function of the distance to each source, the source strengths, and the source spacing. VGRIDns allows the spacing for all of the sources to be multiplied by a user-defined input (ifact), which is in general equal to unity. To create the coarse grid, the baseline grid sources were used but with the source sizes increased by $\sqrt{(2)}$. This led to approximately 9×10^4 faces on the surface of the aircraft and a total of 2.85×10^6 cells (mixed tetrahedrons and prisms). The viscous spacing and growth rate were left unchanged compared to the baseline mesh. For the fine grid the source sizes on the aircraft surface were divided by $\sqrt{(2)}$ with the outer boundary spacing left unchanged. This resulted in

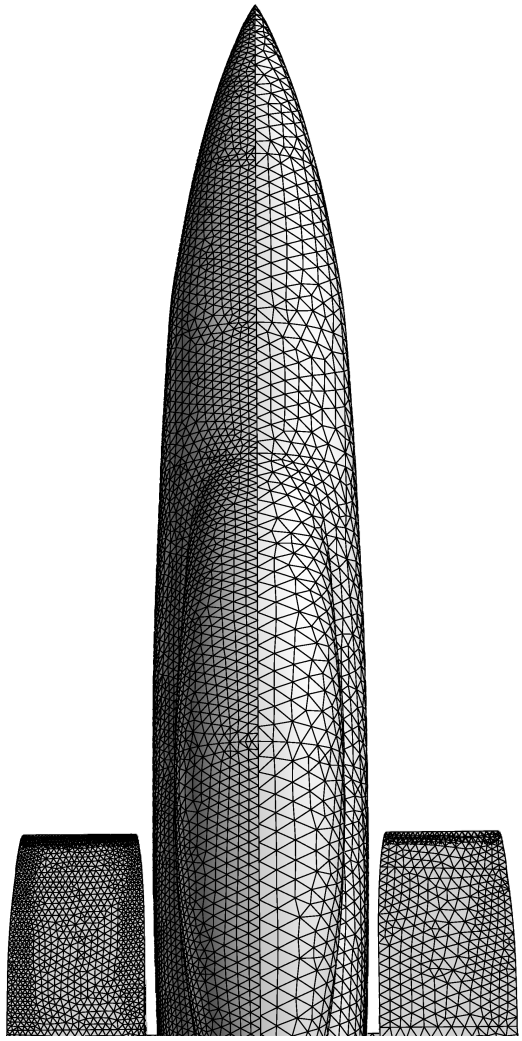

Fig. 3 Surface meshes on the nose for the coarse grid (2.85×10^6 cells) and fine grid (10.0×10^6).

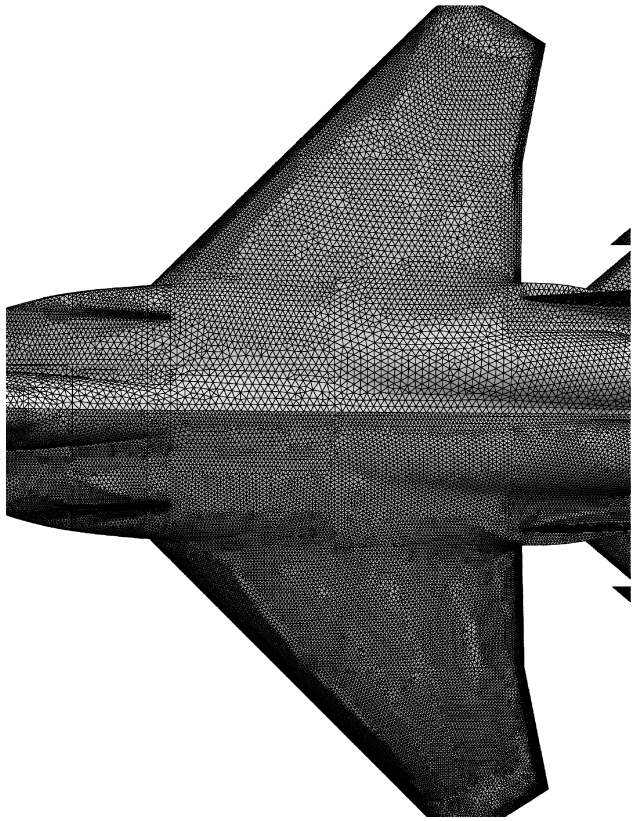

Fig. 4 Surface meshes on the wing for the coarse grid (2.85×10^6) and fine grid (10.0×10^6).

Fig. 5 Surface meshes on the tail for the coarse grid (2.85×10^6) and fine grid (10.0×10^6).

approximately 2.2×10^5 faces on the aircraft surface and 10×10^6 cells (mixed tetrahedrons and prisms). The geometric cell growth rate in the wall-normal direction was reduced from 1.30 to 1.25 for the fine grid. This relatively straightforward procedure provided a systematic approach to examining grid sensitivity in the complex configuration considered in this work.

Results

The computations were performed of the flow over a clean F-15E with no control deflections at $\alpha = 65$ deg and zero sideslip. Boeing provided the authors with a stability and control database for the F-15E that was developed from a comprehensive spin testing program (courtesy of Ken Walck and Glen Peters of Boeing Military). Two stable spin conditions are detailed, including data for symmetric and asymmetric fuel loads. The aircraft with symmetric loading maintains a stable spin at 65-deg angle of attack; the principle aim of the computations reported in this work to first assess the overall computational approach at the same fixed angle of attack as for the stable spins. All simulations were performed at the following flight-test conditions: a Mach number of 0.3 and standard day 30,000 ft. This resulted in a chord-based Reynolds number of 13.6×10^6.

Preliminary unsteady RANS calculations did not not exhibit any substantial unsteadiness. Consequently, the RANS predictions presented in this manuscript are of the steady-state flow computed using global time stepping and a maximum CFL of 10^6 to give the most efficient convergence to steady state.

The S-A model just outlined was employed in the RANS calculations. All DES results were performed with a nondimensional time step of 0.014 (made dimensionless using the mean chord and freestream velocity), based on the results of the time-step study. Because of the tight clustering in the boundary layer at high Reynolds number, this led to a maximum CFL of over 500,000. The CFL outside the boundary layer was on the order of unity, as recommended by Spalart.[14] The RANS treatment of the boundary layers suppresses the development of flow instabilities (eddy content), and therefore large CFL numbers in the RANS region should not be problematic if the flow solver can stably integrate the discretized system.

Side-by-side comparisons of DES and RANS predictions across the symmetry plane are shown in Fig. 6. The contours and isosurfaces of vorticity are an example in a complex configuration of the feature-resolving capacity of DES in its LES mode, resolving the unsteady, geometry-dependent eddies over the aircraft.

A time-step study was conducted using the baseline grid to assess the temporal characteristics of the DES predictions. Nondimensional time steps of 0.007, 0.014, and 0.028 were used in simulations performed for 28 nondimensional time units (i.e., 4000, 2000, and 1000 time steps, respectively).

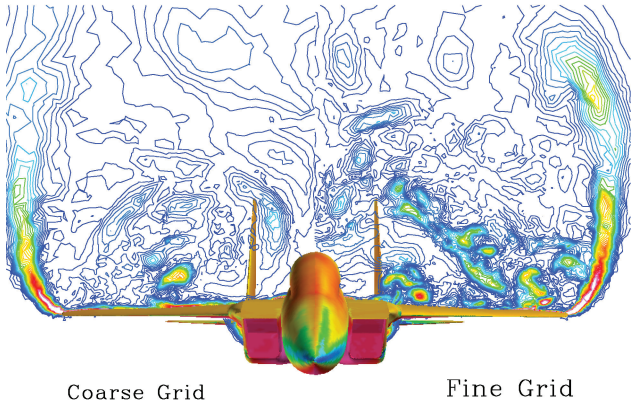

Fig. 6 Vorticity contours along a section of the F-15E from the baseline-grid calculations. Aircraft surface colored by pressure: DES predictions in right-half plane, and S-A results in the left-half plane.

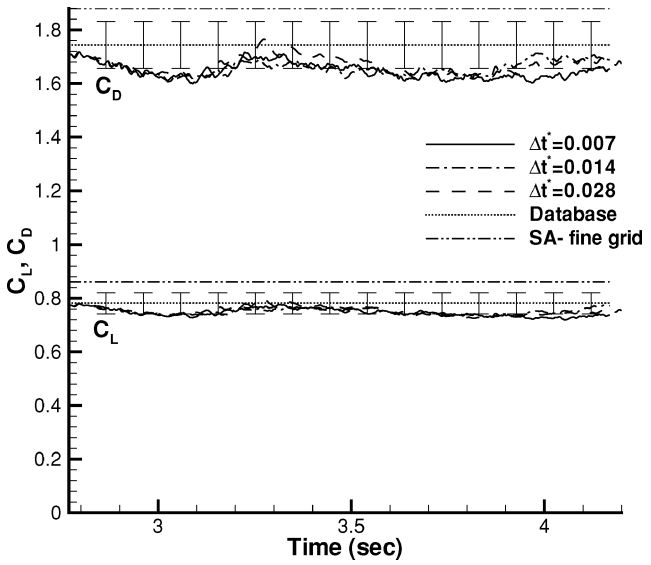

Fig. 7 Convergence history of DES runs on the baseline grid at three time steps compared to the stability and control database values (with 5% error bars) and converged Spalart–Allmaras RANS values.

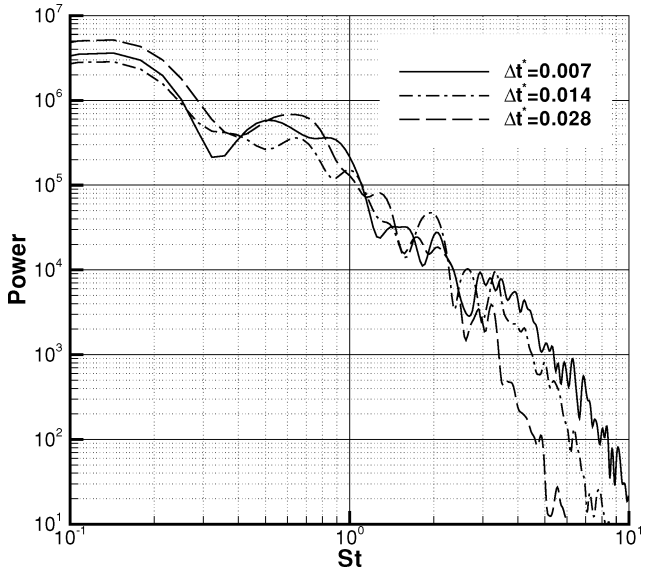

Fig. 8 Frequency spectra of the normal force, baseline-grid computation.

Lift and drag coefficients vs time are plotted in Fig. 7 for the DES time-step study vs the RANS calculation on the fine grid and the stability and control database values. Five-percent error bars have been added to the database values to reflect the expected uncertainty at these conditions. A oscillation of the forces of about 10% is seen in the DES calculations, while the RANS case converged to steady state (not shown). The effect of time step on the solution is difficult to discern using only the force histories.

Frequency spectra of the normal force are plotted in Fig. 8. For each of the time steps, there is a reasonably broad range of frequency content, providing evidence of LES resolution. The largest time step (0.028) begins to fall below the spectra obtained using the finer time steps at about a Strouhal number of three, corresponding to about 12 time steps per cycle. Spectra for the calculation using the intermediate timestep begin to roll off at a Strouhal number closer to six (i.e., again roughly 12 time steps per cycle). For the results that follow, the intermediate time step was used given that it provided a balance between computation time and accuracy.

The effect of mesh resolution on instantaneous properties of the DES predictions are shown in Figs. 9 and 10. The flow visualizations are obtained from the coarse and fine grids. Shown in Fig. 9 are surface streamlines (black), vortex cores (grey), and separation lines (red) along the forebody for the two grids. (The forebody surface is colored by pressure.) The coarse grid appears to be underresolved with a slightly weaker secondary separation. The vortical structure developing from the primary separation is also less coherent as

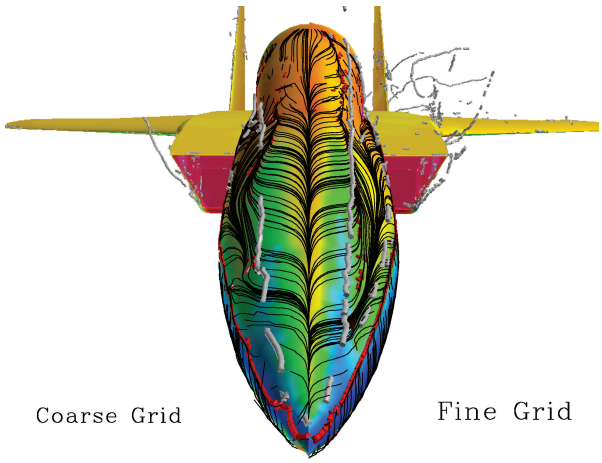

Fig. 9 Instantaneous surface flows and separation line prediction along the forebody and off-body vortex cores: coarse-grid prediction in left-half plane and fine-grid prediction in right-half plane.

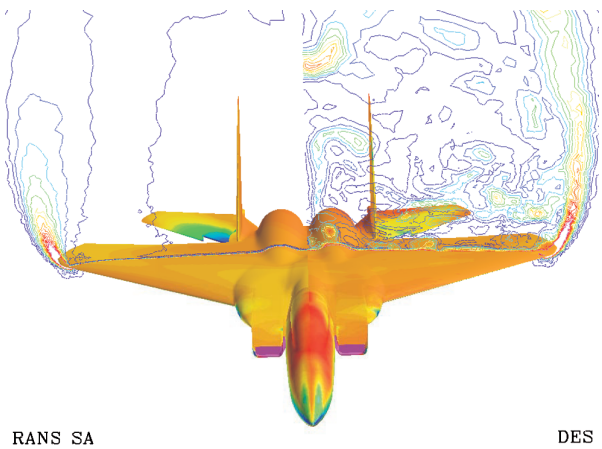

Fig. 10 Contours of the instantaneous vorticity at 680 in. (12.272 m) behind the aircraft reference point with instantaneous pressure plotted on the aircraft surface: coarse-grid prediction in left-half plane and fine-grid result in right-half plane.

Table 1 Averaged lift, drag, and moment coefficients

Model	Grid	C_L	C_D	C_M
Database		0.781	1.744	−0.466
DES	Coarse	0.747	1.677	−0.431
	Medium	0.736	1.616	−0.495
	Fine	0.759	1.648	−0.457
S-A	Coarse	0.855	1.879	−0.504
	Medium	0.852	1.867	−0.523
	Fine	0.860	1.880	−0.507

Table 2 Percentage errors in lift, drag, and pitching moment

Model	Grid	$\%C_L$	$\%C_D$	$\%C_M$
DES	Coarse	−4.25	−3.86	−7.62
	Medium	−5.70	−7.35	6.10
	Fine	−2.81	−5.52	−2.00
S-A	Coarse	9.49	7.73	8.17
	Medium	9.09	7.05	12.22
	Fine	10.22	7.78	8.72

indicated by the separation and reattachment lines. One view of the resolution of the unsteady flow features is accomplished by examination of the vorticity in a cutting plane shown in Fig. 10. The LES character of DES will yield a wider range of scales as grid spacings are reduced, an effect that is apparent in the figure. Note that even the coarse grid resolves at least some unsteady eddy content—with a few small structures visible above the wing.

The time-averaged drag, lift, and moment coefficients along with the corresponding percentage errors compared to the Boeing database are summarized in Tables 1 and 2. The S-A RANS are relatively accurate in the mean, an interesting finding given the model is applied to prediction of a flow far from its calibration range. Note that for the current configuration at high angle of attack the prediction of flow separation is somewhat less difficult than at lower α. This feature lessens modeling error and assists in obtaining more accurate predictions. The S-A results show little sensitivity to grid refinement, with the exception of the pitching moment. DES predictions exhibit more variation with the grid, some of which can be an indicator of the need to acquire statistics over longer sampling intervals. In general, Table 2 shows that the DES predictions are more accurate with respect to the flight-test data, with percentage errors smaller by as much as a factor of two in the drag coefficient predictions, for example. The largest discrepancy for both simulation techniques occurs in the moment coefficient, which is overpredicted (in a negative sense) by about 8–12% in the S-A results. Viewed in light of the expected accuracy of the Boeing database for this angle of attack around 5%, the DES predictions are certainly satisfactory. Any further improvements would be within the estimated error and would not necessarily indicate a more accurate method. The values summarized in Tables 1 and 2 were obtained from simulations of the half-aircraft configuration (i.e., with reflection conditions imposed on the solution in the symmetry plane). Sensitivity to the domain was assessed using DES predictions of the flow around the full aircraft. The mesh for the full aircraft was obtained by mirroring the half-aircraft grids about the symmetry plane, yielding a mesh of 11.8×10^6 cells. The lift and drag coefficients differed by less than 2% compared to those obtained on the half-aircraft grid.

In an effort to understand the source of the differences between the RANS and DES predictions with grid refinement, the pressure coefficient from the (steady-state) RANS is compared to the time average of the DES predictions. Sections are taken on the forebody, wing, and horizontal stabilizer. Relatively significant changes with both grid refinement and simulation technique are observed on the forebody in Figs. 11 and 12. In the figures $\theta = 0$ deg is on the windward plane of symmetry, whereas $\theta = 180$ deg is in the leeward plane of symmetry. The first peak in C_p on this curve at $\theta = 110$ deg occurs as the flow negotiates the shoulder of the forebody, similar to the peak suction observed for flows over cylinders at supercritical Reynolds numbers.

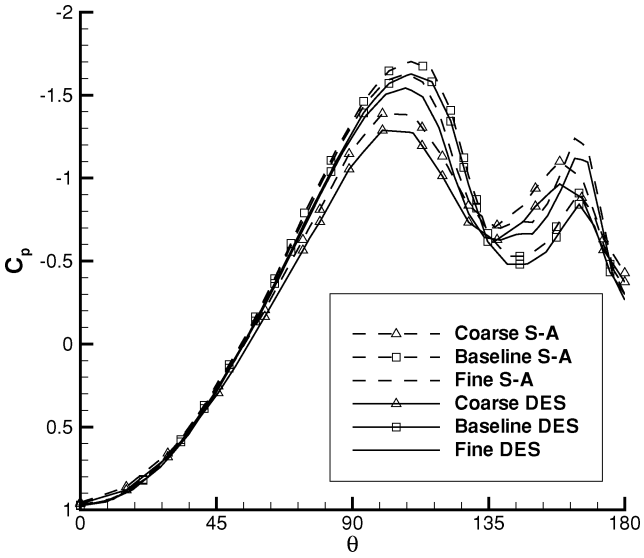

Fig. 11 Pressure coefficients on the F-15E forebody, 200 in. (5.08 m) from the aircraft datum.

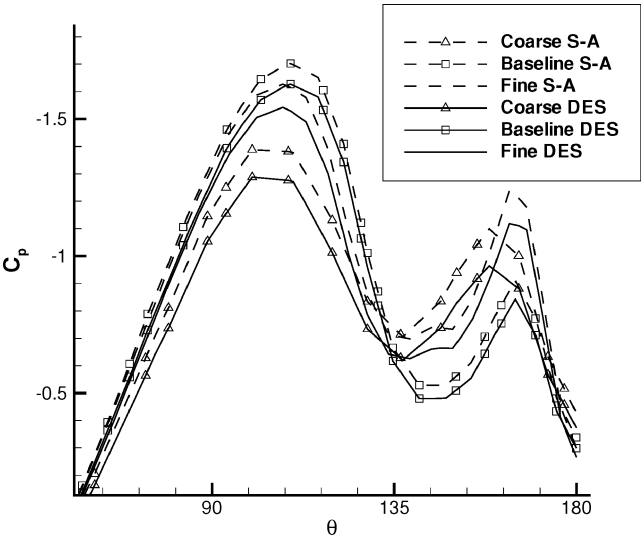

Fig. 12 Pressure coefficients on the F-15E forebody, 200 in. (5.08 m) from the aircraft datum.

The second peak occurs underneath the vortex that develops in the aft region of the forebody. RANS and DES show increases in the peak suction with refinement from the coarse to the fine grid. The baseline grid, however, has a stronger peak suction rounding the shoulder and a weaker vortex (as measured by the second peak in C_p) for both the RANS and the DES when compared to the fine grid. One contributor could potentially be caused by the fact that the fine grid employed a lower geometric growth rate in the boundary layer, perhaps subtly changing the separation characteristics. The overall trend with grid refinement, however, is as expected: stronger vortices (deeper suction peaks) as the grid is refined with improvements in resolution of vortical motions.

Figure 13 suggests that both DES and RANS yield a grid-converged solution for the flow over the wing. DES predicts a relatively uniform pressure that is the norm on a wing with separation, while the RANS results shows more variation in C_p. Overall, however, the RANS results are not far from the DES predictions, unlike solutions of canonical flows such as that around a two-dimensional NACA airfoil at high angle of attack.[7] The relatively strong coherent vortex shedding around two-dimensional shapes such as an airfoil or circular cylinder remains problematic for RANS because of the inability of these models to accurately account for, among

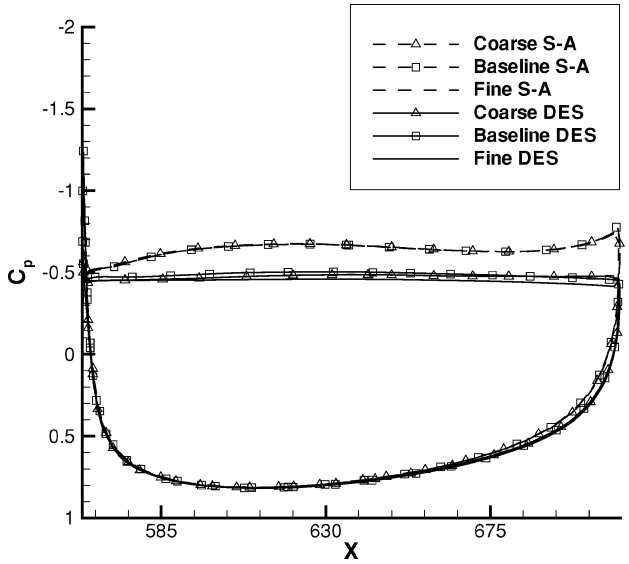

Fig. 13 Pressure coefficients on the F-15E wing, 158 in. (4.0132 m) from the aircraft centerline.

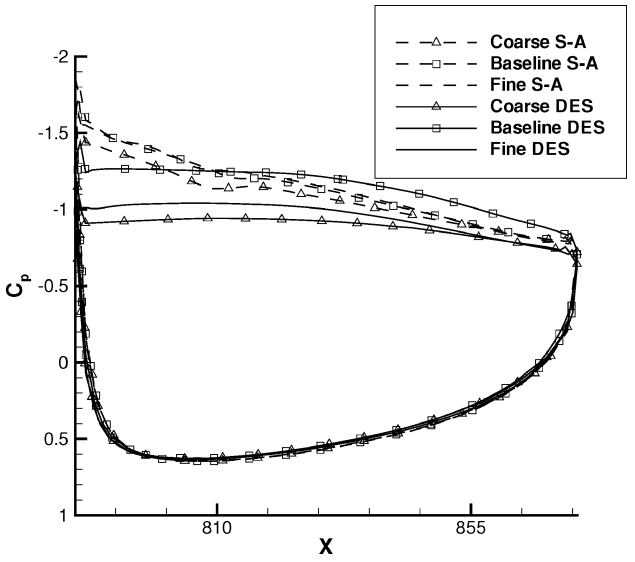

Fig. 14 Pressure coefficients on the F-15E horizontal stabilizer, 120 in. (3.048 m) from the aircraft centerline.

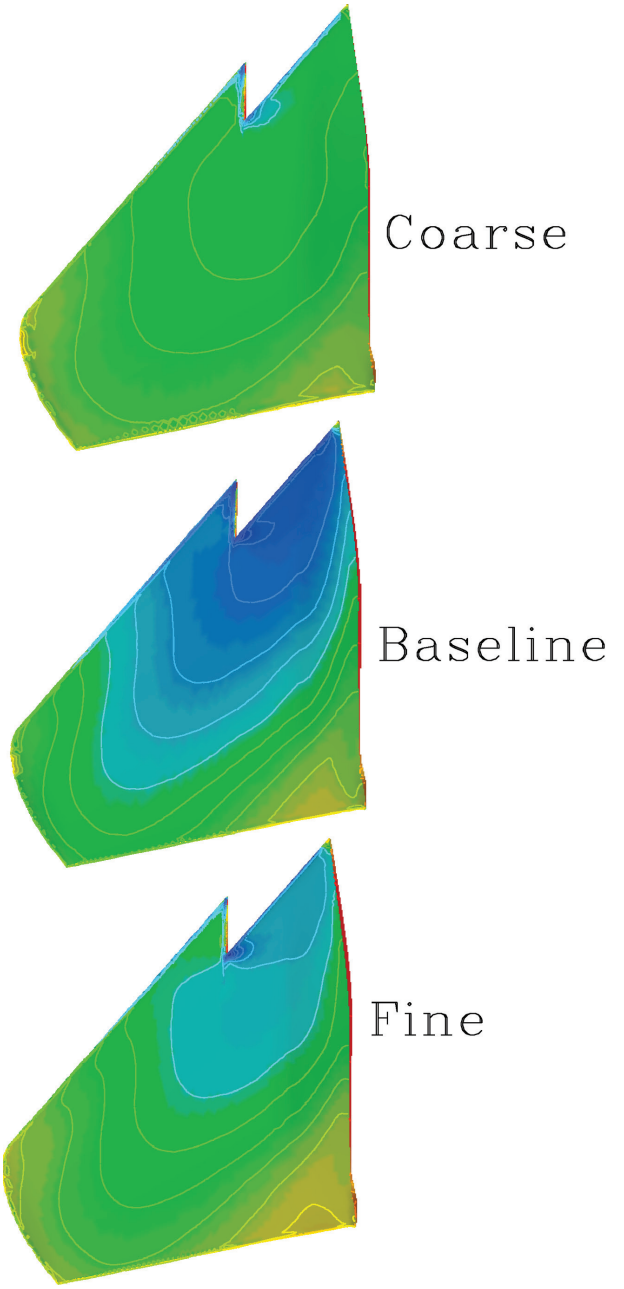

Fig. 15 Time-averaged contours of DES predictions of the pressure on the horizontal stabilizer for the three grids.

other features, the modulation in vortex shedding. The flow over the F-15E appears not as strongly dominated by coherent shedding over a limited frequency band, lessening the need for RANS models to account for features such as force modulation.

The pressure coefficient on the horizontal stabilizer shows more significant changes with variations in model and grid resolution, as shown in Fig. 14. The differences between the baseline and fine grids for RANS are virtually identical, suggesting a grid-converged solution. The DES results for the baseline grid differ significantly from both the coarse and fine grids. Contours of the time-averaged pressure coefficient from the DES over the entire horizontal stabilizer are plotted for the three grids in Fig. 15. Although Fig. 14 makes it appear that the coarse and fine grids are yielding similar solutions, Fig. 15 shows that the surface pressures around the sawtooth are quite different. One explanation could be in the nature of DES: as a coarse grid is refined, the eddy viscosity can drop below the level required for an accurate RANS result, though the grid might still not be sufficient for supporting eddy content and therefore developing sufficient resolved turbulent stresses. Thus, it is possible that a solution can deteriorate and then improve with grid refinement. Another potential source of error is the small temporal sample that was used for time averaging the forces and flow variables. In the absence of any experimental data or a grid-converged solution on the horizontal stabilizer, it is difficult to determine the cause of the reversal. Figure 16 presents instantaneous contours of vorticity for the baseline and fine grids. The fine grid seems to be much improved over the baseline grid in its capacity to provide sufficient resolution of three-dimensional eddy structure in the LES region. Note that because these are instantaneous images, it is difficult to comment on flow topology such as the presence of a tip vortex in the baseline calculation. This tip vortex is likely caused by the presence of crossflow that might come and go with time.

Overall it appears that although the predictions do not exhibit uniform grid convergence across the domain for either RANS or DES the overall forces are not strongly sensitive to grid refinement over the range examined. The lift and drag show small variations for each technique, likely because the wing is well resolved and the flow at high angle of attack. The larger variations in pitching

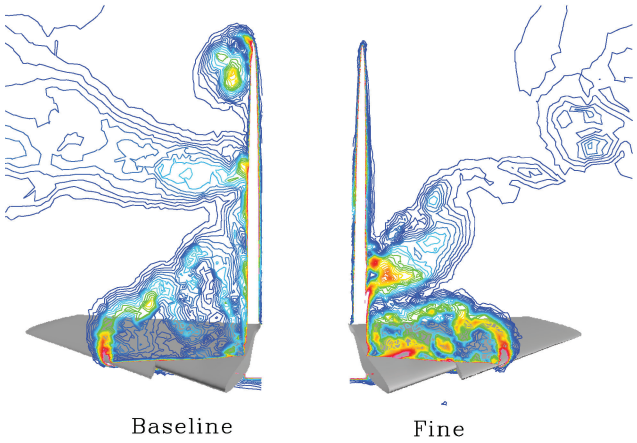

Fig. 16 Contours of the instantaneous vorticity in the tail region.

moment are caused by the variations in pressure on the nose and horizontal stabilizer, which have a stronger effect on the moment because of the long moment arm for these regions of the geometry.

The adequate performance in the RANS was somewhat surprising given the accuracy problems faced by RANS in massively separated flows in canonical geometries such as a two-dimensional NACA airfoil at similar angle of attack.[7] Other configurations such as the two-dimensional flow around circular cylinders are also difficult to predict using RANS.[2] In other massively separated flows, however, such as that around a sphere, RANS predictions are adequate.[15] The three-dimensional character of the flow over the F-15E can assist RANS in providing a reasonable description of the mean. That aspect, combined with the fact that separation prediction is less a challenge than at lower angles of attack, assists in lessening modeling errors, perhaps contributing to the adequate performance reported in this manuscript.

Summary

For the F-15E the present DES are probably one of the first applications of a turbulence-resolving technique to full aircraft at flight Reynolds numbers in which turbulent boundary layers on the vehicle were represented without recourse to wall functions (i.e., with surface-normal grid spacings within one viscous unit at the wall). Both DES and RANS were subjected to a range of grid refinement of approximately a factor of two in each coordinate direction near the surface of the aircraft. The RANS results showed strong evidence of grid convergence in the overall forces. DES predictions showed slightly more sensitivity to grid refinement, although pressures on the wing are essentially grid converged. Pressure distributions on the forebody, wing, and horizontal stabilizer suggest that the horizontal stabilizer and forebody are slightly underresolved. One outcome of these observations is motivation for the use of adaptive gridding. Computation of the full aircraft had little effect on the integrated forces compared to the half-aircraft simulations. A time-step study was performed in the DES showing a reasonable resolution of the LES content of the solution with the baseline time step. The CPU cost of DES vs steady RANS was approximately seven times higher on the same grid.

The predicted lift, drag, and pitching moments from both RANS and DES were accurate in terms of their agreement with the Boeing database, with DES yielding slightly superior predictions. The adequate performance in the RANS was somewhat surprising given the accuracy problems faced by RANS in massively separated flows in canonical geometries such as a two-dimensional NACA airfoil at similar angle of attack.[7] Other configurations such as the two-dimensional flow around circular cylinders are also difficult to predict using RANS.[2] In other massively separated flows, however, such as that around a sphere, RANS predictions are adequate.[15] The three-dimensional character of the flow over the F-15E can assist RANS in providing a reasonable description of the mean. That aspect, combined with the fact that separation prediction is less a challenge than at lower angles of attack, assists in lessening modeling errors, perhaps contributing to the adequate performance reported in this manuscript. However, although global quantities such as lift, drag, and moment were reasonable, RANS predictions failed to produce any significant unsteadiness in the computed solutions, whereas DES resolved a wider range of length and timescales as the grid density was increased. This would be a positive development in extensions of DES to areas such as aeroelasticity and aeroacoustics. Application of DES to these and other areas will further stress numerical treatments, requiring higher fidelity from the underlying numerical schemes, among other factors. The cost of the DES simulations was roughly seven times more than a steady RANS simulation in this case on the same grid.

Acknowledgments

The authors gratefully acknowledge the support of U.S. Air Force Office of Scientific Research Grant F49620-00-1-0050 (Program Manager: Tom Beutner). The authors are also grateful for the assistance of Glen Peters, Ken Walck, and Walt Labozzetta of Boeing Military, who provided the stability and control database and the F-15E geometry. Misha Strelets provided results and grids from his group's NACA 0012 calculations. Matthieu Chapelet and Kory Klismith have assisted with grid generation and postprocessing. Warren Carroll and Alan VantLand aided in postprocessing the F-15E results. Computer support for the computations was provided by the Naval Oceanographic Office Major Shared Resource Center and the Maui High Performance Computing Center.

References

[1]Spalart, P. R., Jou, W. H., Strelets, M., and Allmaras, S. R., "Comments on the Feasibility of LES for Wings, and on a Hybrid RANS/LES Approach," *First AFOSR International Conference on DNS/LES, in Advance in DNS/LES*, edited by C. Liu and Z. Liu, Greyden Press, Columbus, OH, 1997.

[2]Travin, A., Shur, M., Strelets, M., and Spalart, P. R., "Detached-Eddy Simulations Past a Circular Cylinder," *Flow, Turbulence, and Combustion*, Vol. 63, Jan. 2000, pp. 293–313.

[3]Strang, W. Z., Tomaro, R. F., and Grismer, M. J., "The Defining Methods of Cobalt$_{60}$: a Parallel, Implicit, Unstructured Euler/Navier–Stokes Flow Solver," AIAA Paper 99-0786, Jan. 1999.

[4]Tomaro, R. F., Strang, W. Z., and Sankar, L. N., "An Implicit Algorithm for Solving Time Dependent Flows on Unstructured Grids," AIAA Paper 97-0333, Jan. 1997.

[5]Spalart, P. R., and Allmaras, S. R., "A One-Equation Turbulence Model for Aerodynamic Flows," *La Recherche Aerospatiale*, No. 1, 1994, pp. 5–21.

[6]Spalart, P. R., "Strategies for Turbulence Modeling and Simulations," *International Journal of Heat and Fluid Flow*, Vol. 21, pp. 252–263.

[7]Shur, M. L., Spalart, P. R., Strelets, M. K., and Travin, A. K., "Detached-Eddy Simulation of an Airfoil at High Angle of Attack," *Proceedings of the 4th International Symposium on Engineering Turbulence Modelling and Measurements*, edited by W. Rodi and D. Laurence, Elsevier, Amsterdam, May 1999, pp. 669–678.

[8]Gottlieb, J. J., and Groth, C. P. T., "Assessment of Riemann Solvers for Unsteady One-Dimensional Inviscid Flows of Perfect Gases," *Journal of Computational Physics*, Vol. 78, No. 2, 1988, pp. 437–458.

[9]Karypis, G., Schloegel, K., and Kumar, V., "ParMETIS: Parallel Graph Partitioning and Sparse Matrix Ordering Library Version 1.0," Univ. of Minnesota, Dept. of Computer Science, Minneapolis, MN, July 1997.

[10]Grismer, M. J., Strang, W. Z., Tomaro, R. F., and Witzemman, F. C., "Cobalt: A Parallel, Implicit, Unstructured Euler/Navier–Stokes Solver," *Advances in Engineering Software*, Vol. 29, No. 3–6, 1998, pp. 365–373.

[11]Squires, K. D., Forsythe, J. R., and Spalart, P. R., 2001, "Detached-Eddy Simulation of the Separated Flow Around a Forebody Cross-Section," *Direct and Large-Eddy Simulation IV*, ERCOFTAC Series, Vol. 8, edited by B. J. Geurts, R. Friedrich, and O. Metais, Kluwer Academic, Norwell, MA, pp. 481–500.

[12]Forsythe, J. R., Hoffmann, K. A., Cummings, R. M., and Squires, K. D., "Detached-Eddy Simulation with Compressibility Corrections Applied to a Supersonic Axisymmetric Base Flow," *Journal of Fluids Engineering*, Vol. 124, No. 4, 2002, pp. 911–923.

[13]Pirzadeh, S., "Three-Dimensional Unstructured Viscous Grids by the Advancing Layers Method," *AIAA Journal*, Vol. 34, No. 1, 1996, pp. 43–49.

[14]Spalart, P., "Young-Person's Guide to Detached-Eddy Simulation Grids," NASA CR 2001-211032, July 2001.

[15]Constantinescu, G., Chapelet, M., and Squires, K. D., "On Turbulence Modeling Applied to Flow over a Sphere," AIAA Paper 2000-0540, Jan. 2000.